Chemical Engineering Journal 184 (2012) 176–183

Contents lists available at SciVerse ScienceDirect

Chemical Engineering Journal

journal homepage: www.elsevier.com/locate/cej

Adsorbent ability of lignin-based activated carbons for the removal of *p*-nitrophenol from aqueous solutions

Luis M. Cotoruelo[a,*], María D. Marqués[a], Francisco J. Díaz[a], José Rodríguez-Mirasol[a], Juan J. Rodríguez[b], Tomás Cordero[a]

[a] Departamento de Ingeniería Química, Facultad de Ciencias, Universidad de Málaga, 29071 Málaga, Spain
[b] Ingeniería Química, Facultad de Ciencias, Universidad Autónoma de Madrid, 28049 Madrid, Spain

ARTICLE INFO

Article history:
Received 16 October 2011
Received in revised form
23 December 2011
Accepted 3 January 2012

Keywords:
p-Nitrophenol
Activated carbon
Adsorption
Equilibrium
Thermodynamics
Kinetics

ABSTRACT

This paper reports the *p*-nitrophenol (PNP) removal from aqueous solutions by adsorption onto active carbons (ACs). Nine ACs were prepared from acid-precipitated eucalyptus kraft lignin following a two-step process consisting in CO_2 partial gasification (750–850 °C) after carbonization (350–800 °C) in N_2 atmosphere. The amount adsorbed ranged from 1 to 4.4 mmol/g, and it is related to the initial concentration of adsorbate, temperature, pH, burn off of the activated carbons, and contact time. The equilibrium results were fitted by the Temkin, Dubinin-Radushkevich, and Guggenheim-Anderson-de Boer equations. The main thermodynamic magnitudes were estimated as well, and their values indicated that the adsorption processes were spontaneous and exothermic. The kinetic study showed that the processes are of apparent second order related to the concentrations of the empty active sites on the ACs surface. The values of the effective diffusivities have been calculated and they have suggested that the internal diffusion controls the net mass transfer. The results obtained in the present work can be for the benefit of the preparation of new adsorbents, as well as the primary design of the adsorption equipment with separation or environmental purposes.

1. Introduction

Progressive increases in the industrial activity produce large amounts of toxic compounds. Among them, *p*-nitrophenol (PNP) can enter the environment during the production of dyes, pesticides and drugs. Nitrophenols are toxic to plants and animals. Due to its harmful effects, wastewaters containing phenolic compounds must be treated before to their discharge to the receiving water bodies. Many different types of adsorbent may be evaluated to remove substituted phenols from wastewaters. They include, among others, XAD polymeric resins [1] and activated carbons, which still are the adsorbents widest used to this end [2–12]. On the other hand, as we have reported in previous works [13,14], the preparation of activated carbons from kraft lignin is an interesting possibility for the lignin benefit as an alternative way for the black liquors from the cellulose pulp industry, as they are usually processed. So, the objective of this work has been to study the adsorption of PNP from aqueous solutions using ACs prepared in our laboratory. The ACs derived from eucalyptus kraft lignin have been chosen for their valuable properties based on their well developed surface area, surface chemical nature, and their thermo-chemical stability. Also, the use of PNP adsorption from water or organic (benzene, heptane, and xylene) solutions became a referenced procedure in the surface study of varied adsorbents, as alumina, carbons, cement, metal powders, silica, titania, pigments, sugar, and wool [15–17].

2. Materials and methods

The experimental procedures followed in the preparation and characterization studies of the ACs as adsorbents (here named as: A40, B20, B40, C50, D40, E4, E12, E16, and E20) were previously described in detail elsewhere [18]. The raw material was eucalyptus kraft lignin supplied by the Empresa Nacional de Celulosas as obtained by acid precipitation of kraft black liquors. This lignin was carbonized under N_2 atmosphere and then it was activated by partial gasification with CO_2 during different times to obtain activated carbons with different burn off.

The porous structures of the ACs were characterized by means of adsorption–desorption of N_2 at 77 K and CO_2 at 273 K using a Quantachrome apparatus (Autosorb-1 model) and mercury porosimetry using a Carlo Erba mercury porosimeter 4000. Ultimate analyses of the ACs were carried out in a Perkin-Elmer (model 2400 CHN) analyzer.

* Corresponding author. Tel.: +34 952132037; fax: +34 952132038.
E-mail address: lcot@uma.es (L.M. Cotoruelo).

1385-8947/$ – see front matter © 2012 Elsevier B.V. All rights reserved.
doi:10.1016/j.cej.2012.01.026

Table 1
Preparation conditions and final properties of the ACs.

AC	A40	B20	B40	C50	D40	E4	E12	E16	E20
A_{BET} (m^2/g)[a]	1450	1123	1343	1319	1613	822	1273	1348	1853
A_S (m^2/g)[b]	725	354	510	373	367	36	341	393	504
$V_{microp.\ CO_2}$ (cm^3/g)[c]	0.380	0.354	0.366	0.372	0.384	0.304	0.339	0.351	0.376
$V_{microp.\ N_2}$ (cm^3/g)[d]	0.528	0.426	0.567	0.510	0.576	0.331	0.483	0.531	0.701
$V_{mesop.}$ (cm^3/g)[e]	0.992	0.714	0.740	0.490	0.770	0.060	0.480	0.780	0.860
$V_{macrop.}$ (cm^3/g)[f]	0.510	0.189	0.343	0.240	0.310	0.020	0.110	0.150	0.530
Carbonization temp. (K)	550	800	800	350	350	350	350	350	350
Activation temp. (K)	800	800	800	750	800	850	850	850	850
Activation time (h)	40	20	40	50	40	4	12	16	20
Burn off (%)[g]	66.7	54.8	71.3	67.3	70.5	21.3	54.5	63.5	76.8
Yield (% weight)	14.5	17.8	11.3	12.7	11.3	31.5	18.2	13.9	9.4
Ultimate analyses (% dry ash free basis)									
C (%)	92.8	96.4	94.5	93.1	94.5	95.5	94.8	94.3	93.7
O (%)	6.65	2.88	4.98	6.21	4.87	3.92	4.69	5.23	5.86
H (%)	0.55	0.72	0.52	0.69	0.63	0.58	0.51	0.47	0.44
Inorganic material (%)	12.1	7.5	10.2	8.2	11.0	4.2	6.8	8.5	11.2

[a] Determined by adsorption of N_2 at 77 K (BET equation with $A_m = 0.162\ nm^2$).
[b] External surface determined from the N_2 adsorption isotherm by α_S method.
[c] Determined by adsorption of CO_2 at 273 K (Dubinin-Radushkevich equation).
[d] Determined from the N_2 adsorption isotherm by α_S method.
[e] (From 2 to 8 nm width) estimated from the N_2 adsorption isotherm by taking volume adsorbed at $P/P_o = 0.950$ as liquid and (from 8 to 50 nm width) estimated by mercury porosimetry by taking cumulative pore volume at $r = 25$ nm.
[f] Estimated by mercury porosimetry by taking cumulative pore volume.
[g] Calculated as the sample weight loss relative to completely devolatilized kraft lignin.

For the liquid phase adsorption, a previous experimentation included a program for the influences of the initial concentration of PNP, as well as the adsorbent dose. An adsorbent dose of 0.100 g AC/L (dry basis), and a range from 50 to 300 mg PNP/L were set as selected for the tests in this present work. So, the equilibrium and the kinetic experiments were carried out by putting the doses of activated carbon weighted into glass flasks. A stock solution of PNP (Merck, 99.5% purity) was prepared in distilled water and the desired concentrations were obtained by successive dilutions. 100 mL of aqueous solutions of different initial concentrations (C_o: 0.036–2.157 mmol/L) were added to the glass flasks to contact the ACs, and mechanically agitated at 180 rpm using an orbital incubator (Gallenkamp, model INR-250). The samples were kept at different test temperatures in the range 283 K–313 K. The contact times varied between 10 and 14 days (depending on the samples). The solutions from the kinetic tests were analyzed for different contact times up to 2 h. To analyze the PNP concentrations, a calibration plot was prepared by measuring the absorbance of samples with different predetermined concentrations (UV–vis spectrophotometer Varian, model Cary 1E, λ_{max}: 315 nm). To avoid the pH influence on the absorbance of the samples, all samples were previously acidified by adding 0.1 M HCl.

3. Results and discussion

3.1. Characterization of the activated carbons

Eucalyptus kraft lignin is not a porous material ($A_{BET} < 1\ m^2/g$) as supplied, and it has no adsorption capacity as is. A first thermochemical process is necessary to develop any specific surface area, and it has to be followed by a physical activation. A high grade of porosity (microporosity and a certain grade of mesoporosity) is developed by the activation process. The resulting ACs have heterogeneous physical and chemical structure. The former arises from the existence of pores with different sizes. The latter is originated from a variety of functional groups (mainly in the form of carbon–oxygen) on the surface. Table 1 summarizes some of the characteristics of the ACs, which have been extensively discussed in a previous work [18]. The surface area and the micropore volume substantially increase with burn off; a widening of micropores, and an increasing mesopores contribution are observed and, at high burn off levels, a significant development of macroporosity can be detected. E series includes ACs with low, intermediate, and high activation degrees. The chemical nature of the ACs surface has been also studied and reported in a previous work [19]. XPS and TPD analyses suggested that the surface oxygen groups formed during gasification were the following: hydroxyl, ether, carbonyl, carboxylic acid, lactones, phenols, quinone, and anhydrides of carboxylic acids.

3.2. Adsorption equilibrium isotherms

3.2.1. Equilibrium results

The adsorption isotherm is an expression for the variation of the adsorbent adsorption capacity (q_e, mmol/g) which is in equilibrium with the concentration of adsorbate (C_e, mmol/L) in the bulk of the solution at a constant temperature.

Graphical presentations of the PNP adsorption isotherms on all ACs at 293 K are depicted in Fig. 1. Fig. 1b displays the E series isotherms for the ACs prepared when the activation time varied. The shape of the isotherms indicates a high adsorbent affinity to the PNP at low concentrations. The isotherms are concave (favorable) with respect to the C_e-axis for the entire concentration range studied. The highest adsorption capacities corresponded to D40 and E20, in agreement with their highest total surface development. The adsorbed amount progressed with the increase of the AC burn off, as a consequence of the greater surface area and mesoporosity development. The isotherm of E20 revealed a high adsorption capacity even at low equilibrium concentrations. In contrast, the E4 isotherm provided a weak enlarge on its capacity values toward the highest PNP concentrations in the solution.

To have an idea about the expected yield from the adsorption system, it is important at first, to establish the most appropriate correlations for the equilibrium state curves. Various isotherm equation types like those from Guggenheim-Anderson-de Boer (GAB), Dubinin-Radushkevich (D-R) and Temkin, have been tested to describe the equilibrium data.

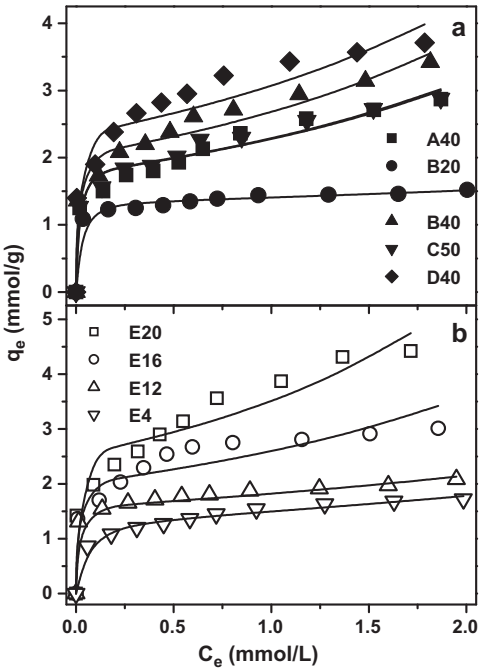

Fig. 1. Experimental data (dots) and GAB fits (curves) for the adsorption isotherms of PNP on ACs at 293 K: (a) A40, B20, B40, C50, and D40; (b) E series.

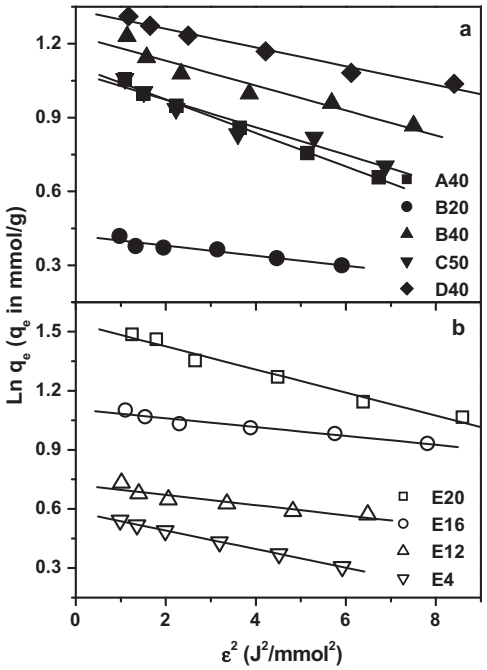

Fig. 2. Experimental data (dots) and D-R fits (linear) for the adsorption isotherms of PNP on ACs at 293 K: (a) A40, B20, B40, C50, and D40; (b) E series.

3.2.2. Guggenheim-Anderson-de Boer model

The GAB model [20] may be expressed as:

$$q_e = \frac{K_1 M_{GAB} C_e}{(1 - K_2 C_e)(1 + (K_1 - K_2)C_e)} \quad (1)$$

where K_1 and K_2 (L/mmol) are the isotherm constants and M_{GAB} (mmol/g) is the equilibrium concentration of adsorbate on the solid phase corresponding to a complete coverage of the adsorption sites. This equation can become a Langmuir isotherm for $K_2 = 0$. Fig. 1 and Table 2 show the results of the fits to the GAB model (included the values of χ^2: average quadratic deviation).

3.2.3. Dubinin-Radushkevich model

The D-R equation [21] is expressed as:

$$q_e = M_{D\text{-}R} \exp(-\beta\varepsilon^2) \quad (2)$$

Eq. (2) can be linearized as:

$$\text{Ln } q_e = \text{Ln } M_{D\text{-}R} - \beta\varepsilon^2 \quad (3)$$

where $M_{D\text{-}R}$ (mmol/g) represents the theoretical saturation capacity; β ($mmol^2/J^2$) is a constant related to the adsorption energy; and ε (J/mmol) is the Polanyi potential, which is related to the equilibrium concentration as follows:

$$\varepsilon = RT \text{ Ln}\left[1 + \left(\frac{1}{C_e}\right)\right] \quad (4)$$

where R is the gas constant (0.008314 J/mmol K) and T is the absolute temperature (K). The Polanyi sorption potential (ε) is the work required to remove a molecule from its location in the sorption space to infinity, independent of the temperature. This model assumes the heterogeneity of sorption energies within this space. The values of $M_{D\text{-}R}$ and β may be estimated by plotting Ln q_e vs. ε^2; i.e., from the intercept and the slope of the straight lines depicted by Eq. (3). Table 2 shows the results of the fits to the D-R equation and the values of r^2 (determination coefficient). Experimental data and their D-R fits are plotted in Fig. 2.

Table 2
GAB, D-R and Temkin isotherm constants at 293 K and coverage factors.

AC	A40	B20	B40	C50	D40	E4	E12	E16	E20
GAB									
M_{GAB} (mmol/g)	1.783	1.333	2.057	1.789	2.373	1.399	1.586	2.025	2.556
K_1 (L/mmol)	302.0	104.1	362.9	315.9	354.2	156.8	222.9	331.5	395.7
K_2 (L/mmol)	0.217	0.061	0.232	0.218	0.238	0.088	0.131	0.220	0.269
χ^2	2.9E-2	4.9E-3	2.7E-2	2.1E-2	5.2E-2	3.4E-2	1.3E-2	6.2E-2	9.9E-2
D-R									
$M_{D\text{-}R}$ (mmol/g)	3.031	1.523	3.428	2.956	3.804	1.795	2.061	3.019	4.674
β ($mmol^2/J^2$)	0.068	0.020	0.051	0.056	0.038	0.058	0.022	0.026	0.047
r^2	0.995	0.915	0.925	0.939	0.977	0.999	0.970	0.947	0.977
E (J/mmol)	2.71	5.00	3.13	2.99	3.63	2.94	4.77	4.39	3.26
Temkin									
M_T (mmol/g)	0.620	0.138	0.632	0.544	0.605	0.299	0.201	0.435	1.029
K_T (L/mmol)	51.60	2.9 E4	100.1	94.25	255.6	170.8	1.2 E4	599.1	42.66
b ($J\,g/mmol^2$)	3.927	17.644	3.853	4.476	4.025	8.144	12.114	5.598	2.366
r^2	0.967	0.960	0.969	0.957	0.995	0.989	0.967	0.943	0.983
Equivalent area occupied and coverage factors for C_o: 2.157 mmol/L									
A_{PNP} (m^2/g_{AC})	907	480	1082	910	1173	544	658	952	1398
C.F. (A_{PNP}/A_{BET})	0.63	0.43	0.81	0.69	0.73	0.66	0.52	0.71	0.75

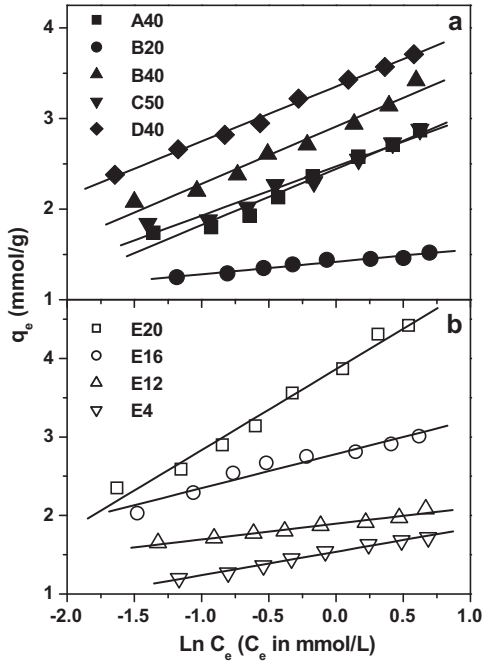

Fig. 3. Experimental data (dots) and Temkin fits (linear) for the adsorption isotherms of PNP on ACs at 293 K: (a) A40, B20, B40, C50, and D40; (b) E series.

The constant β gives the mean adsorption free energy (E) when the adsorbate is transferred from the infinity in the solution to the surface of the solid. It can be calculated as:

$$E = \frac{1}{\sqrt{2\beta}} \tag{5}$$

The magnitude of E (J/mmol) is useful for estimating the mechanism of the adsorption step (Table 2). In the present case, with $E < 8$ kJ/mol, it is assumed that the physical forces are the main affecting the adsorption mechanism.

3.2.4. Temkin model

The Temkin isotherm [21] describes the behaviour of the adsorption systems on heterogeneous surfaces. This model assumes that: (1) the adsorption heat of all the molecules in the layer decreases linearly with the coverage due to the adsorbate–adsorbate interactions and (2) the adsorption is characterized by a homogeneous distribution of binding energies, up to some maximum binding energy. The Temkin equation may be expressed as:

$$q_e = \left(\frac{RT}{b}\right) \mathrm{Ln}(K_T C_e) \tag{6}$$

If $RT/b = M_T$; then Eq. (6) can be linearized as:

$$q_e = M_T \ \mathrm{Ln}\, K_T + M_T \,\mathrm{Ln}\, C_e \tag{7}$$

where K_T (L/mmol) is the binding equilibrium constant corresponding to the maximum binding energy, and M_T (mmol/g) is related to the heat of adsorption. A plot of q_e vs. Ln C_e makes possible the determination of M_T and K_T from the slope and intercept, respectively. Table 2 and Fig. 3 show the results of the fits to the Temkin equation and the values of r^2.

The values of the equivalent area occupied (A_{PNP}), as well as the corresponding coverage factor (C.F.: A_{PNP}/A_{BET}) reached at the maximum initial concentration used (C_o: 2.157 mmol/L) have been calculated. According to Eq. (8), any q_e value can be transformed to PNP equivalent surface area (A_{PNP}) which would cover 1 g of AC assuming that the PNP molecules take a parallel orientation (flat adsorption) on the AC surface and the surface area covered by each molecule adsorbed is 52.5 Å^2 [15]:

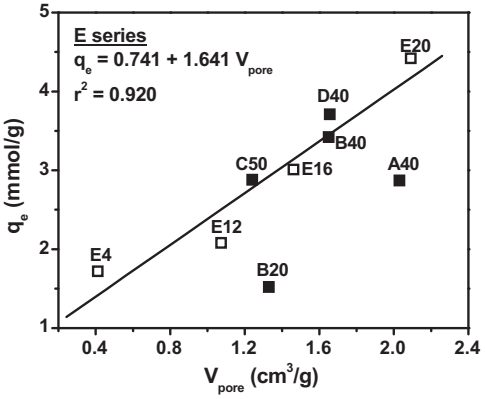

Fig. 4. Amount of PNP adsorbed as function of the ACs total pore volume.

$$A_{PNP}\left(\frac{m^2_{PNP}}{g_{AC}}\right) = 316.2\left(\frac{m^2_{PNP}}{\mathrm{mmol}_{PNP}}\right)\cdot q_e\left(\frac{\mathrm{mmol}_{PNP}}{g_{AC}}\right) \tag{8}$$

Table 2 shows the values of the coverage factors for the PNP adsorption. Those are in the range from 40 to 80% of the BET specific surface areas. When comparing the different ACs (except E4 with E12), we have observed that the coverage factors increase as burn offs increase. This is the consequence of the activation grade influence, as combination of the micro and mesoporosity developed.

Fig. 4 shows the maximum adsorption capacity (C_o: 2.157 mmol/L) of PNP vs. the total pore volume for all the studied ACs. A linear-like trend has been obtained for E series; it confirms the favorable effect of the activation step. E4 has a very low capacity (1.720 mmol/g) while E20 shows a very high capacity (4.420 mmol/g). This is in agreement with their internal surface area development, and more especially with the volume of mesopores.

3.3. Effect of the pH on the adsorption

The adsorption of PNP at different pH (from 3 to 11) is depicted in Fig. 5. The removal of PNP was the maximum at acid pH, but it was slightly decreasing, and when the pH of the solution increased to values higher than 7, especially up to alkaline, the adsorption of PNP decreased sharply.

PNP (a water soluble solid) is moderately acid in water ($pK_a = 7.15$). When the solution pH is acid; for example pH = 2; then: [*p*-nitrophenol]/[*p*-nitrophenolate] = 1.4×10^5, almost all the

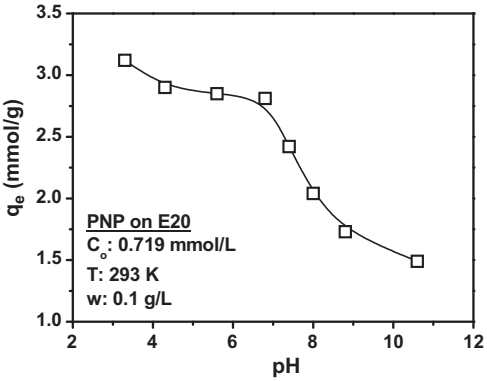

Fig. 5. pH effect on the adsorption equilibrium of PNP.

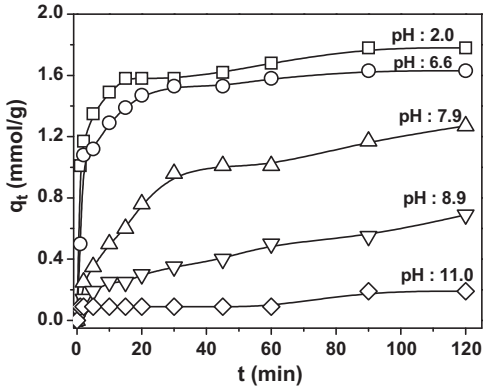

Fig. 6. Kinetic of PNP adsorption on E16 at different pH. C_o: 0.719 mmol/L; T: 293 K; w: 0.100 g/L.

molecules of PNP in solution are in their molecular form. At low pH, there is nearly no electrostatic repulsion; so, the adsorbed amount is the maximum. The largest amount adsorbed at low pH may be the result of the strong chemical bond between the lonely pair of electrons on the hydroxyl group in PNP and the surface of AC, as well as the existing forces from the dispersive interactions between the aromatic ring of the PNP and specific sites on the activated carbon surface. At high pH values, the PNP molecules are more ionized to *p*-nitrophenolate anions; the number of negatively charged sites increases and the number of positively charged sites decreases. The surface groups on the AC become anionic (negative charge), as carboxilate (—COO^-) and phenolate (Ph—O^-) ions, and they are not favorable for the adsorption of anions. So, the sharp decrease in the adsorption capacity at basic pH may be attributed to the electrostatic repulsion between the *p*-nitrophenolate molecules and the negatively charged adsorbent surface. Moreover, the low adsorption at high pH is probably due to the presence of OH^- ions competing with the phenolates for the residual positively charged adsorption sites on the ACs surface.

As a complementary study, the kinetic adsorption data for PNP on E16 at different pH have been obtained (Fig. 6). It can be observed that at low pH, the adsorption capacity and the rate increase as a consequence of the occurring strong attraction forces. Nevertheless, it may not be practical to maintain extreme pH values because it would need addition of chemicals to lower the pH and the effluent would need a final neutralization step before its discharge.

3.4. Effect of the temperature on adsorption

The temperature influences the adsorption equilibrium and its variations produce a displacement from or toward the phase adsorbed. Also, an increase in temperature generally improves the solubility of the molecules (if in liquid phase) and their diffusion within the pores of the adsorbent materials. Fig. 7 shows the adsorption capacity of B20 and E12 at different temperatures. The isotherms show similar behaviours, with strong affinities of the PNP molecules for the surfaces, as evidenced by the initial slopes. The amounts adsorbed of PNP rose with the decrease of the temperature, indicating the apparent exothermic nature of the entire process. Similar effect has been reported by other authors [6,22–24]. In general, physical adsorption processes are typically exothermic; an increase in temperature causes a reaction in the opposite direction, i.e., this produces desorption of molecules from the less energetic active centres, resulting a displacement in the equilibrium toward the fluid phase. The thermodynamic analysis provides information about the process ability to take place and the stability of the adsorbed phase as well. The changes on the free energy (ΔG) have been estimated at 293 K for all the ACs, and at

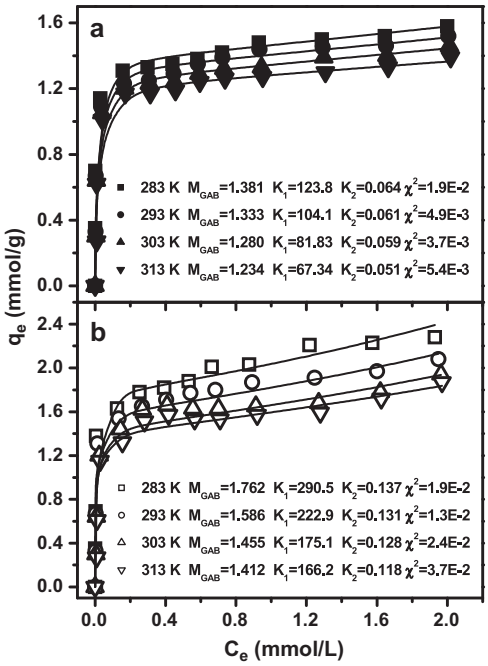

Fig. 7. Experimental data (dots) and GAB fits (curves) for the adsorption isotherms of PNP at different temperatures: (a) B20; (b) E12. M_{GAB} in (mmol/g), K_1, K_2 in (L/mmol).

four temperatures for B20 and E12. In addition, for these latter ACs, the enthalpy (ΔH) and the entropy (ΔS) changes have been also calculated.

The free energy of adsorption has been calculated from the expression derived from the Gibbs adsorption equation [25]. If we refer the free energy change per mol of solute adsorbed, the following final expression can be obtained:

$$\Delta G = -\frac{RT}{q_e}\int_0^{C_e}\frac{q_e}{C_e}dC_e \tag{9}$$

where q_e is related to C_e by the adsorption isotherm. In the present work, as a criterion, the fits of the GAB equation have been used for the calculation of the equilibrium relations. The ΔG values (kJ/mol) have been calculated using Eq. (9) by numerical integration. In this case, ΔG depends on the temperature and the grade of coverage (q_e). Table 3 shows the values of ΔG at various levels of surface coverage (C_e: 0.800, 1.200, and 2.000 mmol/L). The negative values of ΔG indicate the feasibility of the processes and the spontaneous nature of the PNP adsorption on all the ACs. Although the increase in C_e induces a higher amount adsorbed in the equilibrium, we have found that, in some of cases, the absolute values of ΔG get lower. At high C_e, the average released energy descends when covering a great variety of more and less active sites. By contrast, for B20, E4 and E12, with low burn off, A_{BET}, and porosity developed, ΔG increases (average molar values) a little when C_e increases. It seems that it is a consequence of their active sites distribution for adsorption, which has to take place on the most active sites, mainly located the microporosity places inside. On the other hand, B20 and E12 have showed a little or negligible increase in ΔG when the temperature decreased. These complex phenomena are due to the adsorbents surface heterogeneity as well as the variety of possible combined mechanisms to organize and to drive the mass transfer steps.

Table 3
Thermodynamics for adsorption at different equilibrium concentrations. C_e (mmol/L), T (K), ΔG and ΔH (kJ/mol), ΔS (J/mol K).

AC	T	C_e = 0.800				C_e = 1.200				C_e = 2.000			
		ΔG	ΔH	ΔS	$T_{(\Delta G=0)}$	ΔG	ΔH	ΔS	$T_{(\Delta G=0)}$	ΔG	ΔH	ΔS	$T_{(\Delta G=0)}$
A40	293	−11.1				−10.9				−9.4			
B20	283	−9.3	−16.1	−24	671	−10.0	−15.6	−20	780	−10.6	−13.4	−10	1340
	293	−9.0				−9.7				−10.4			
	303	−8.7				−9.5				−10.3			
	313	−8.6				−9.4				−10.3			
B40	293	−15.9				−15.0				−12.2			
C50	293	−11.5				−11.3				−9.7			
D40	293	−19.8				−18.3				−14.5			
E4	293	−5.9				−6.6				−7.3			
E12	283	−5.4	−7.1	−5.9	1203	−6.0	−7.0	−3.4	2059	−6.4	−6.9	−1.9	3632
	293	−5.3				−5.9				−6.4			
	303	−5.3				−5.9				−6.3			
	313	−5.2				−5.9				−6.3			
E16	293	−16.0				−15.2				−12.6			
E20	293	−24.7				−22.3				−16.2			

The enthalpy and the entropy changes for the adsorption of PNP on B20 and E12 in a range of temperature between 283 K and 313 K have been estimated by the Gibbs–Helmholtz equation:

$$\Delta G = \Delta H - T\Delta S \tag{10}$$

The values ΔH and ΔS have been determined from the intercept and the slope, respectively, by plotting ΔG vs. T (Fig. 8). The negative values of ΔH confirm the exothermic nature of the overall process (Table 3). Contrary to ΔG, the absolute values of ΔH decreased a little as the coverage level grew. This situation is frequent in the adsorption on non-homogeneous surfaces. It can be explained because the process is easier on the surface sites at low coverage level, attending to energy reasons. The fits from Eq. (10) have determined negative values of ΔS which result from a lower grade of freedom of the molecules in the adsorbed phase than in the fluid phase. In these cases ($\Delta H < 0$; $\Delta S < 0$), the process can only occur when $|T\Delta S| < |\Delta H|$. The process has to become exothermic enough to overtake the disadvantage due to the negative change of entropy. If the temperature value is enough high, the term $T\Delta S$ can surpass the term ΔH, and the process does not take place. The highest values of T for the different cases analyzed according to a spontaneous process have been reported as $T_{(\Delta G=0)}$ in Table 3.

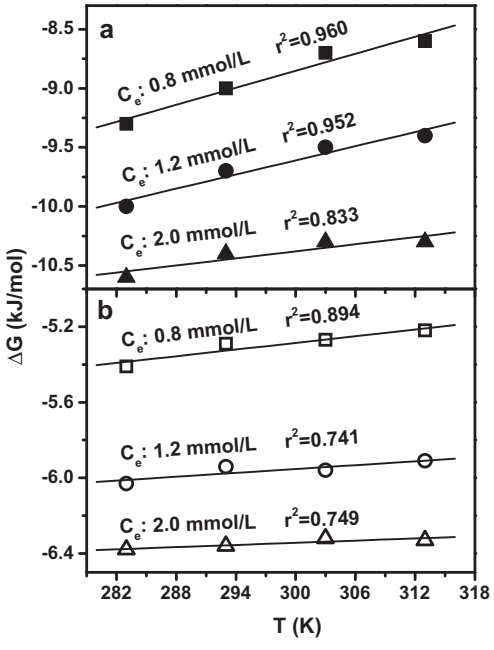

Fig. 8. Thermodynamic estimations for the adsorption of PNP on B20 and E12 at different surface coverage: (a) B20; (b) E12.

Nevertheless, the low accuracy obtained from the simplicity of Eq. (10) as used, with its linear regressions, allow thinking that these results are numerical estimations and relative trends for the thermodynamic magnitudes and their dependence on the variables. One of these relates to the porous structure of the adsorbents, because its accessibility in energy terms varies as the adsorption takes place. Therefore, the values calculated for ΔG, ΔH and ΔS may represent the apparent behaviours associated with the adsorption processes as they have been studied; at the interval of temperatures and the other experimental conditions set.

3.5. Kinetic study

3.5.1. Empirical model for the fluid phase

The solid–liquid adsorption processes on porous materials may be described as a series of steps: external mass transfer from the liquid phase to the solid surface through the boundary layer, internal diffusion within the porous particle, and adsorption on the surface. For the present study, the results from D40 and E12 were selected as examples, on the basis of their surface properties and adsorptive behaviours.

The amount q_t (mmol/g) of PNP adsorbed on the AC was calculated as the change in the aqueous phase concentration from the initial value by:

$$q_t = \frac{C_o - C_t}{w} \tag{11}$$

where C_t (mmol/L) is the adsorbate concentration at a certain contact time t. At the sight of the shape of the kinetic plots for D40 and E12, as showed in Fig. 9, an empirical model was used for the adsorbate concentration decay curves in the aqueous phase. The experimental results for the PNP adsorption were fitted to the following second order exponential decay equation:

$$C_t = y_o + A_1 \exp(-B_1 t) + A_2 \exp(-B_2 t) \tag{12}$$

$$\frac{dq_t}{dt} = \frac{A_1 B_1}{w} \exp(-B_1 t) + \frac{A_2 B_2}{w} \exp(-B_2 t) \tag{13}$$

where y_o, A_1, B_1, A_2, and B_2 are empirical coefficients. Their values are shown in Fig. 9. The plot attached to Fig. 9 shows the values derived from Eq. (13). It is observed a sharp decrease in the adsorption rate during the first minutes of contact time. This step

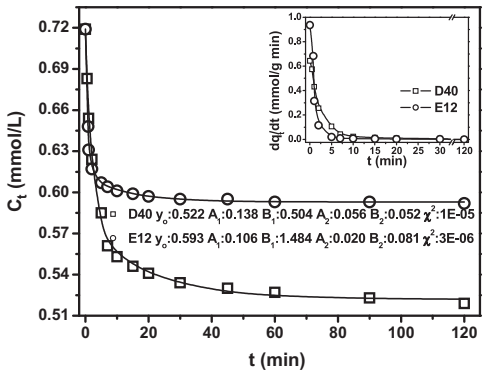

Fig. 9. Experimental data (dots) and fits (curves) for kinetic of PNP adsorption on D40 and E12. C_o: 0.719 mmol/L; T: 293 K; w: 0.100 g/L. y_o, A_1, A_2 in (mmol/L); B_1, B_2 in (min^{-1}).

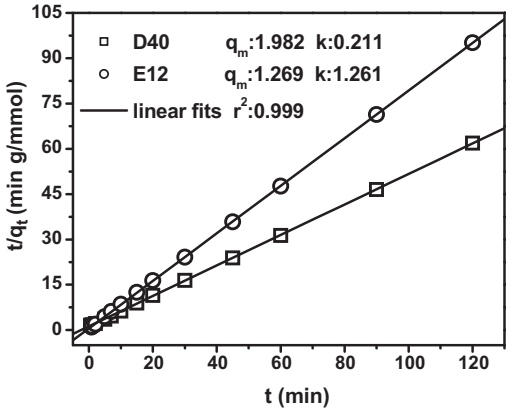

Fig. 10. Kinetic order plots for PNP adsorption on D40 and E12. C_o: 0.719 mmol/L; T: 293 K; w: 0.100 g/L; q_m in (mmol/g); k in (g/mmol min).

corresponds to the surface coverage in the widest pores and the most active sites. A second step develops for 15 min approximately with an intermediate decreasing rate. This step is the most interesting to the kinetic control for its relation to the coverage into the narrow mesopores and micropores. The last part developed a negligible adsorption rate which leads to the equilibrium concentrations, so extended as several days of contact time. The adsorption rate was higher on D40 than on E12. It can be explained because of the first's higher surface area and pore volume (Table 1).

3.5.2. Kinetic model for the solid phase

The kinetic data have been analyzed by the Lagergren model [26] for order n; it is:

$$\frac{dq_t}{dt} = k(q_m - q_t)^n \tag{14}$$

where k is the adsorption rate constant referred to the adsorbate concentration on the solid, n is the apparent order of the process related to the available adsorbent concentration $(q_m - q_t)$, which is the driving force of the process, that is, the vacant and accessible active sites in the surface of the adsorbent, for any time of contact. In this work, q_m (mmol/g) represents the asymptotic q_t value in the function in the given experimental conditions. However, the selected equation (with its parameters evaluated for 120 min of contact time) cannot be used to predict the equilibrium concentrations (data as far as 8–12 days). The values of q_m may be calculated as:

$$q_m = \frac{C_o - y_o}{w} \quad \{\text{D40} : 1.97\,\text{mmol/g} \quad \therefore \quad \text{E12} : 1.26\,\text{mmol/g}\} \tag{15}$$

In addition, by integration of Eq. (14) for $n = 2$, we have [27]:

$$\frac{t}{q_t} = \frac{1}{kq_m^2} + \frac{1}{q_m}t \tag{16}$$

The values of k (g/mmol min) and q_m, can be obtained from the intercept and the slope of the straight lines in the plots (t/q_t vs. t; Fig. 10). The values (q_t, t) were those supplied by the experimental fittings of the decay model. The linear regressions from Eq. (16) were acceptable, and they provided q_m values very close to those from Eq. (15), which verify the applicability of this kinetic equation for an apparent second order in the adsorption process of PNP.

3.5.3. Effective diffusion coefficients

A number of models to think about the main mass transfer resistances (external and internal diffusion) have been postulated, which differ in their description of the diffusion process into the pores [28].

The diffusion process in the homogeneous sphere model can be expounded by means of an equation involving constant diffusivity, that is to say, a single parameter, effective or apparent that we will denominate D_i; what is representative of all the positions into the particle. This approach avoids to differentiate among diffusion in the pore spaces (pore diffusion), diffusion across the surfaces which can occur subsequent to adsorption (surface diffusion), and diffusion in the solid material itself. Crank [29] developed the following equation for spherical particles:

$$\frac{q_t}{q_e} = 1 - \frac{6}{\pi^2}\sum_{n=1}^{\infty}\frac{1}{n^2}\ \exp\left(\frac{-D_i n^2 \pi^2 t}{R_P^2}\right) \tag{17}$$

where R_P is the radius of the adsorbent particle.

This equation provides and exact solution for the situation often described as "infinite bath", which assumes a constant surface concentration for the solute, and a negligible external film resistance. For short times (St), or more precisely: $q_t/q_e < 0.3$; D_i becomes D_{St}, and Eq. (17) may be approximated to:

$$D_{St} = \left(\frac{q_t}{q_e}\right)^2 \frac{\pi R_P^2}{36t} \tag{18}$$

For "long times" (i.e. Lt; D_{Lt}), the highest terms in the series of Eq. (17) become extremely small, and only the first term has prevalence. We have

$$D_{Lt} = \frac{R_P^2}{\pi^2 t}\,\text{Ln}\left[\frac{6/\pi^2}{1 - (q_t/q_e)}\right] \tag{19}$$

Due to mathematical reasons D_{Lt} values only may be positive if $(q_t/q_e) > [1 - (6/\pi^2)]$. In the present work, we have used Eqs. (18) and (19) to determine the D_i values (D_{St} and/or D_{Lt}) from the kinetic

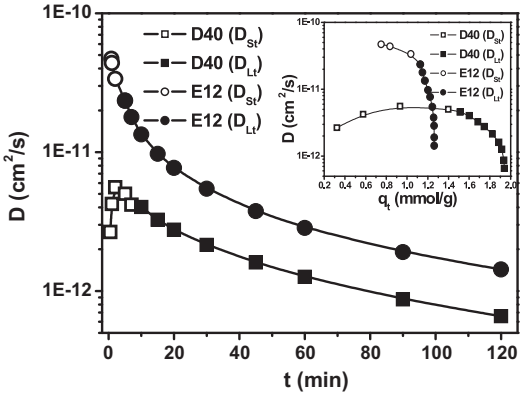

Fig. 11. Effective diffusion coefficients. Variation with the contact time and with the load adsorbed (enclosed).

data showed in Fig. 9. The q_t values corresponding to the different times were supplied by the second order exponential decay model. Fig. 11 plots the effective diffusivity values as a function of the contact time and the amount adsorbed. The equations did not predict constant values. After several minutes of contact time, the apparent diffusion coefficients decreased, according to the increasing difficulty that the molecules find to penetrate into the porous structures. Multiple collisions among molecules and the pore walls, as well as the partial obstruction of the pore mouths can occur as the same time. The surface areas of the pores become gradually less attainable to adsorption.

4. Conclusions

Activated carbons obtained from lignin, at different experimental conditions, have been successfully employed as adsorbents for quantitative removal of PNP from aqueous solution. Chemical and physical characteristics, as surface areas, pore volumes and pore sizes, determine the yields and rates expected for the potential use of the ACs as adsorbents. It has been found that the activated carbons burn off influences on the adsorption capacity. The thermodynamic analysis indicated that the PNP adsorption was spontaneous and exothermic. The results from the sorption energy parameters estimation showed the physisorption nature of the adsorption processes. The kinetic analysis revealed adsorption rates with second apparent order related to the available active sites on the activated carbons surfaces. The effective diffusion coefficients were low, in the range from 10^{-12} to 10^{-10} cm^2/s, decreasing with the time, what suggests that the internal porosity controls the rate of the mass transfer toward the ultimate equilibrium state.

Acknowledgments

The authors acknowledge the Spanish DGICYT-MEC (Project CTQ 2009-14262) and the Junta de Andalucía (TEP-184) for the financial support.

References

[1] K.E. Noll, V. Gounaris, W. Hou, Adsorption Technology for Air and Water Pollution Control, Lewis Pub. Inc., Chelsea, 1992.
[2] A. Wolborska, Adsorption on activated carbon of p-nitrophenol from aqueous solution, Water Res. 23 (1989) 85–91.
[3] C. Moreno-Castilla, J. Rivera-Utrilla, M.V. López-Ramón, F. Carrasco-Marín, Adsorption of some substituted phenols on activated carbons from a bituminous coal, Carbon 33 (1995) 845–851.
[4] S.K. Srivastava, R. Tyagi, Competitive adsorption of substituted phenols by activated carbon developed from the fertilizer waste slurry, Water Res. 29 (1995) 483–488.
[5] R. Leboda, B. Charmas, Evaluation of surface area of carbon component of model carbon-silica adsorbents from adsorption data of *p*-nitrophenol from aqueous solutions, Colloids Surf. A 135 (1998) 267–275.
[6] S. Dutta, J.K. Basu, R.N. Ghar, Studies on adsorption of *p*-nitrophenol on charred saw-dust, Sep. Purif. Technol. 21 (2001) 227–235.
[7] S. Haydar, M.A. Ferro-García, J. Rivera-Utrilla, J.P. Joly, Adsorption of *p*-nitrophenol on an activated carbon with different oxidations, Carbon 41 (2003) 387–395.
[8] A.P. Terzyk, M. Wisniewski, P.A. Gauden, G. Rychlicki, S. Furmaniak, Carbon surface chemical composition in *para*-nitrophenol adsorption determined under real oxic and anoxic conditions, J. Colloid Interface Sci. 320 (2008) 40–51.
[9] M. Ahmaruzzaman, S. Laxmi Gayatri, Batch adsorption of 4-nitrophenol by acid activated jute stick char: Equilibrium, kinetic and thermodynamic studies, Chem. Eng. J. 158 (2010) 173–180.
[10] B. Petrova, B. Tsyntsarskia, T. Budinova, N. Petrova, L.F. Velasco, C.O. Ania, Activated carbon from coal tar pitch and furfural for the removal of *p*-nitrophenol and m-aminophenol, Chem. Eng. J. 172 (2011) 102–108.
[11] S. Suresh, V.C. Srivastava, I.M. Mizar, Adsorptive removal of phenol from binary aqueous solution with aniline and 4-nitrophenol by granular activated carbon, Chem. Eng. J. 171 (2011) 997–1003.
[12] M.B. Hobday, P.H.Y. Li, D.M. Crewdson, S.K. Bhargava, The use of low rank coal-based adsorbents for the removal of nitrophenol from aqueous solution, Fuel 73 (1994) 1848–1854.
[13] J. Rodríguez-Mirasol, T. Cordero, J.J. Rodríguez, Activated carbons from CO_2 partial gasification of eucalyptus kraft lignin, Energy Fuels 7 (1993) 133–138.
[14] J. Rodríguez-Mirasol, T. Cordero, J.J. Rodríguez, Preparation and characterization of activated carbon from eucalyptus kraft lignin, Carbon 31 (1993) 87–95.
[15] C.H. Giles, A.P. D'Silva, A.S. Trivedi, Use of *p*-nitrophenol for specific surface measurement of granular solids and fibres, J. Appl. Chem. 20 (1970) 37–41.
[16] C.H. Giles, T.H. MacEwan, S.N. Nakhwa, D. Smith, Studies in adsorption. Part XI. A system of classification of solution adsorption isotherms, and its use in diagnosis of adsorption mechanisms and in measurement of specific surface areas of solids, J. Chem. Soc. (1960) 3973.
[17] C.H. Giles, S.N. Nakhwa, Studies in adsorption. XVI. The measurement of specific surface areas of finely divided solids by solution adsorption, J. Appl. Chem. 12 (1962) 266–273.
[18] L.M. Cotoruelo, M.D. Marqués, F.J. Díaz, J. Rodríguez-Mirasol, T. Cordero, J.J. Rodríguez, Activated carbons from lignin: their application in liquid phase adsorption, Sep. Sci. Technol. 42 (2007) 3363–3389.
[19] L.M. Cotoruelo, M.D. Marqués, J. Rodríguez-Mirasol, T. Cordero, J.J. Rodríguez, Adsorption of aromatic compounds on activated carbons from lignin: Equilibrium and thermodynamic study, Ind. Eng. Chem. Res. 46 (2007) 4982–4990.
[20] E.A. Guggenheim, Application of Statistical Mechanics, Clarendon Press, Oxford, 1966.
[21] D.D. Do, Adsorption Analysis: Equilibria and Kinetics, Series on Chemical Engineering, vol. 2, Imperial College Press, London, 1998.
[22] J.M. Chern, Y.W. Chien, Adsorption of nitrophenol onto activated carbon: isotherms and breakthrough curves, Water Res. 36 (2002) 647–655.
[23] D. Tang, Z. Zheng, K. Lin, J. Luan, J. Zhang, Adsorption of *p*-nitrophenol from aqueous solutions onto activated carbon fiber, J. Hazard. Mater. 143 (2007) 49–56.
[24] J.M. Li, X.G. Meng, C.W. Hu, J. Du, Adsorption of phenol, *p*-chlorophenol and p-nitrophenol onto functional chitosan, Bioresour. Technol. 100 (2009) 1168–1173.
[25] J.P. Bell, M. Tsezos, Removal of hazardous organic pollutants by biomass adsorption, J. Water Pollut. Control Fed. 59 (1987) 191–198.
[26] S. Lagergren, About the theory of so-called adsorption of soluble substances (Zur theorie der sogenannten adsorption geloester stoffe), K. Sven. Vetenskapsakad Handl. 24 (1898) 1–39.
[27] Y.S. Ho, C.C. Chiang, Sorption studies of acid dye by mixed sorbents, Adsorption 7 (2001) 139–147.
[28] A. Leitão, E. Conceição, R. Santos, A. Rodrigues, Modelling of solid–liquid adsorption: effect of adsorbent loads on model parameters, Can. J. Chem. Eng. 70 (1992) 690–698.
[29] J. Crank, The Mathematics of Diffusion, Clarendon Press, Oxford, 1975.